Homography-based method for calibrating an omnidirectional vision system

Beiwei Zhang[1] and Youfu Li[2,*]

[1]*School of Information Engineering, Nanjing University of Finance and Economics, Nanjing, China*
[2]*Department of Manufacturing Engineering and Engineering Management, City University of Hong Kong, Hong Kong, China*
**Corresponding author: meyfli@cityu.edu.hk*

Received January 14, 2008; accepted March 31, 2008;
posted April 14, 2008 (Doc. ID 91508); published May 21, 2008

We present a homography-based method for calibrating an omnidirectional vision system with a parabolic mirror. Assuming that the intrinsic parameters of the camera are known *a priori*, we focus on finding the solution for the mirror parameter and its positions. We first estimate the homographic matrix partially using six or more point correspondences. Then the rotation matrix and two components of the translation vector can be estimated. Finally, the remaining parameters are computed. In this method, a closed-form solution for all the variables is obtained using the homographic matrix. Another advantage is the enhanced robustness in implementation via the use of two over-constrained linear systems. Numerical simulations and real data experiments are also performed to validate the proposed algorithm. © 2008 Optical Society of America

OCIS codes: 110.0110, 120.0120, 120.4640, 150.0150, 330.0330.

1. INTRODUCTION

A central catadioptric vision system can be built by combining a parabolic mirror with an orthographic camera, or a hyperbolic mirror with a perspective camera. It has a large field of view (often larger than 180°) with a single effective viewpoint, and hence features many distinct advantages compared with the traditional vision system with narrow field of view. First, the search for correspondences is easier since the corresponding points do not often disappear from the images. Second, a large field of view stabilizes the motion estimation algorithms. Last but not least, more information of the scene can be reconstructed from fewer images. As a result, the central catadioptric system offers great benefits to visual surveillance, three-dimensional modeling of wide environments, robot navigation, etc.

Just like traditional vision, the catadioptric vision needs calibration before a vision task begins. Many techniques have been proposed in the past several decades for the traditional vision [1,2]. However, because of severe distortion of the view and high nonlinearity of the imaging process with the catadioptric camera, those well-established algorithms under the perspective projection model cannot be applied directly. Therefore, many special efforts have been spent on the catadioptric vision system recently. Baker and Nayar [3] and Geyer and Daniilidis [4], respectively, studied the image formation and the projective geometry in a catadioptric vision system. They showed that a central catadioptric projection is equivalent to a two-step mapping via the sphere. Some researchers, e.g., Barreto [5] and Ying and Hu [6], have proposed a unifying projection model for cataoptric, dioptric, and fisheye cameras. With these theories, some calibration constraints and very practical implications can be obtained for the system. For example, a set of linear equations was constructed for the focal lengths and skew factor of a para-catadioptric-like camera with known principal point in Wu *et al.* [7] using the sphere projection model.

Lines projected as conics in the image plane have intensively been used for calibration in the catadioptric camera [8,9]. Mei and Malis [10] presented an algorithm for structure from motion using 3D line projections in a central catadioptric camera. With the images of three lines, Geyer and Daniilidis [11] gave a closed-form solution for focal length, image center, and aspect ratio for skewless cameras and a polynomial root solution in the presence of skew. Barreto and Araujo [12] investigated the projective invariant properties of central catadioptric projection of lines and suggested an efficient method for recovering the image of the absolute conic, the relative pose between the camera and the mirror, and the shape of the reflective surface.

However, the estimation of the conics using imaged points in these algorithms is hard to accomplish, which limits its use in practice. First, only a small part of the arc of the conic is available from the image due to occlusions and curvature, which makes the results unreliable and inaccurate. Second, when multiple lines are projected in the images, it is difficult to distinguish which conic is the image of a given line. Last, the conics are not always line images. They may be the image of lines, circles, or any other curves. Some researchers have tried to solve these problems. For example, Barreto and Araujo [13] and Barreto and Daniilidis [14] have derived some constraints that are necessary for the conic curves to be line images. However, these are not sufficient conditions.

On the other hand, points as important features for the calibration completely overcome the above listed limitations and have been widely used in the catadioptric camera [15,16]. Wu and Hu [17] investigated the projective

geometric invariants of scene points and their image points where the invariant equations for 1D, 2D, and 3D space points were established via cross ratios of space points and the optical axis. The epipolar geometry in terms of a fundamental matrix has been studied for calibrating the central catadioptric camera by several researchers [18–21]. In 2002, Svoboda *et al.* [20] presented the explicit expression and characterization of epipolar geometry within a pair of central catadioptric cameras. Recently, by lifting the 2D image plane to 5D projective space, Barreto and Daniilidis [21] constructed different formulas for the lifted fundamental matrices in a systematic manner and discussed their structures. Micusik and Pajdla [22–24] showed that the epipolar geometry can be estimated from a small number of correspondences by solving a polynomial eigenvalue problem. Their work allowed the use of robust random-sample-consensus (RANSAC) estimation to find the image projection model and the epipolar geometry from tentative correspondences contaminated by mismatches or noise.

Based on the above discussions, we will employ image points rather than lines as features in this work. In practice, the intrinsic parameters, e.g., the focal lengths and principal point of the camera, are not changed as frequently as the extrinsic parameters. Hence, we focus on the motion parameters as well as the mirror parameter of a parabolic camera system, assuming that the intrinsic parameters are known *a priori*. To solve this problem, we make use of the plane-based homographic matrix, given a few point correspondences between the image and a planar pattern. A closed-form solution for all the variables is provided using the homographic matrix, and the optimization process is very fast. Another advantage is the enhanced robustness in implementation through the use of two over-constrained linear systems. We have carried out some numerical simulations and real data experiments to validate the proposed algorithm, and the results are acceptable.

The remainder of this paper is structured as follows. Section 2 presents the projection model for the parabolic camera. We give the calibration algorithm using plane-based homography in Section 3. Some experimental results are shown in Section 4. Finally, we conclude this paper in Section 5.

2. PROJECTION MODEL

We consider a central parabolic camera system that consists of a parabolic mirror and an orthographic camera. Figure 1 shows a sketch of the system, in which the camera is assembled with the mirror so that the rays of the camera are parallel to the mirror symmetry axis. We construct a right-handed coordinate frame for the system whose origin coincides with the focal point of the mirror. The transformation between the mirror frame and the world frame, which is identified as the extrinsic parameters of the system, is described by rotation matrix $\boldsymbol{R}_m$ and translation vector $\boldsymbol{t}_m$.

In such system, the image formation can be divided into two steps: (1) The world points are projected onto the mirror surface by a central projection from the focal point,

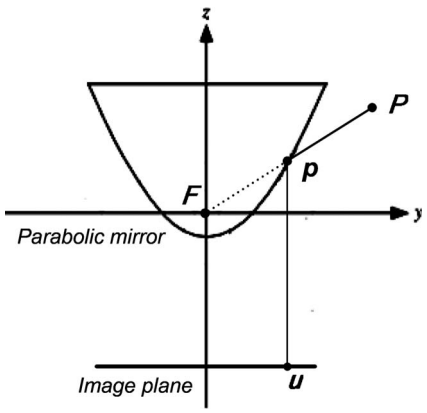

Fig. 1. Parabolic camera system.

(2) the mirror points are orthographically projected into the image plane of the camera.

Let the surface equation of the parabolic mirror be

$$z = \frac{x^2 + y^2 - a^2}{2a}, \tag{1}$$

where a is called the mirror parameter. A point $\boldsymbol{P}$ in the world frame is projected on the mirror surface by a central projection as

$$\boldsymbol{p} = \lambda(\boldsymbol{R}_m\boldsymbol{P} + \boldsymbol{t}_m), \tag{2}$$

where λ is a scale factor. Let $[x\ y\ z]=\boldsymbol{R}_m\boldsymbol{P}+\boldsymbol{t}_m$. Substituting Eq. (2) into Eq. (1), we can obtain the solution for the scale λ as $\lambda = a(z+\sqrt{x^2+y^2+z^2})/x^2+y^2$.

Once λ is determined, the projection from point $\boldsymbol{p}$ to the image point $\boldsymbol{u}$ can be written as

$$\boldsymbol{u} = \alpha\begin{bmatrix}\begin{pmatrix}1 & 0 & 0\\ 0 & 1 & 0\end{pmatrix}\boldsymbol{p}\\ 1\end{bmatrix}, \tag{3}$$

where α is a nonzero scale factor.

On the other hand, if an image point $\boldsymbol{u}$ is known, the corresponding point on the mirror surface can be directly computed as

$$\boldsymbol{p} = \begin{bmatrix} u \\ v \\ \dfrac{u^2 + v^2 - a^2}{2a} \end{bmatrix}, \tag{4}$$

where u and v denote the two components of $\boldsymbol{u}$.

3. CALIBRATING THE CATADIOPTRIC CAMERA

In this work, we assume that the parabolic camera undergoes an arbitrary rigid motion in the scene; so the calibration task then involves determining the mirror parameter and the motion parameters of the system. We will solve these problems by using a homographic matrix in what follows.

A. Homographic Matrix

Assume that $\boldsymbol{P}$ lies on a planar surface and $\boldsymbol{p}$ is its corresponding point on the mirror surface. According to projective geometry, there is a 3×3 homographic matrix $\boldsymbol{H}$ between them satisfying

$$\boldsymbol{p} = \sigma \boldsymbol{H} \boldsymbol{P}, \tag{5}$$

where

$$\boldsymbol{H} = \begin{bmatrix} h_1 & h_2 & h_3 \\ h_4 & h_5 & h_6 \\ h_7 & h_8 & h_9 \end{bmatrix}$$

and σ is a nonzero scale factor.

Without loss of generality, the xy axis of the world frame is assumed to lie on the plane. Hence, the third components of points on that plane are zeros. According to Eqs. (4) and (5), we then have

$$\begin{bmatrix} u \\ v \\ \dfrac{u^2+v^2-a^2}{2a} \end{bmatrix} = \sigma \boldsymbol{H} \begin{bmatrix} x \\ y \\ 1 \end{bmatrix}. \tag{6}$$

In Eq. (6), the unknowns include the mirror parameter a, the scale factor σ, and the homographic matrix $\boldsymbol{H}$. Since it has a special form, we can partially recover the matrix $\boldsymbol{H}$ using some point pairs. From the first two rows, we obtain

$$(h_1x + h_2y + h_3)v - (h_4x + h_5y + h_6)u = 0. \tag{7}$$

We can see that each point pair provides one constraint on the six components of the homographic matrix. Given n pairs of points ($n \geq 6$), we have

$$\boldsymbol{A}\boldsymbol{h} = \boldsymbol{0}, \tag{8}$$

where

$$\boldsymbol{A} = \begin{bmatrix} v_1x_1 & v_1y_1 & v_1 & -u_1x_1 & -u_1y_1 & -u_1 \\ \cdots & \cdots & \cdots & \cdots & \cdots & \cdots \\ v_nx_n & v_ny_n & v_n & -u_nx_n & -u_ny_n & -u_n \end{bmatrix}$$

and $\boldsymbol{h} = [h_1 \quad h_2 \quad h_3 \quad h_4 \quad h_5 \quad h_6]^{\mathrm{T}}$. Using eigenvalue decomposition, the solution for the vector $\boldsymbol{h}$ can be determined up to a scale factor by the eigenvector corresponding to the smallest eigenvalue of $\boldsymbol{A}^{\mathrm{T}}\boldsymbol{A}$.

B. Calibration of the Parabolic Camera

Considering Eqs. (2) and (3), the relationship between the homographic matrix and the extrinsic parameters can be described as

$$s\boldsymbol{H} = \begin{bmatrix} r_{11} & r_{12} & t_1 \\ r_{21} & r_{22} & t_2 \\ r_{31} & r_{32} & t_3 \end{bmatrix}, \tag{9}$$

where s is the scale factor and r_{ij} represents the ijth element of rotation matrix $\boldsymbol{R}_m$ and t_i the ith element of translation vector $\boldsymbol{t}_m$.

Since $\boldsymbol{R}_m$ is an orthogonal matrix, the norm of its 2×2 submatrix should be exactly one. From Eq. (9), the scale factor can be estimated as

$$s = \frac{1}{\mathrm{norm}\left(\begin{bmatrix} h_1 & h_2 \\ h_4 & h_5 \end{bmatrix}\right)}. \tag{10}$$

Then the first 2×2 submatrix of $\boldsymbol{R}_m$ can be determined as

$$R_{11} = sh_1, \quad R_{12} = sh_2, \quad R_{21} = sh_4, \quad R_{22} = sh_5. \tag{11}$$

According to the properties of rotation matrices, the remaining parameters of $\boldsymbol{R}_m$, i.e., R_{13}, R_{23}, R_{31}, R_{32}, and hence R_{33}, can be estimated.

For the translation vector, its first two components are computed as

$$t_1 = sh_3, \quad t_2 = sh_6. \tag{12}$$

Up to now, we have partially recovered the rotation matrix and the translation vector using the homographic matrix. In the next subsection, the remaining motion parameters and the mirror parameters are estimated using the constraints of Eq. (6).

C. Calibrating the Remaining Parameters

From the first and third rows in Eq. (6), we have

$$(h_1x + h_2y + h_3)\frac{u^2+v^2-a^2}{2a} - (h_7x + h_8y + h_9)u = 0. \tag{13}$$

Rearranging Eq. (13), we obtain

$$k^1a^2 + 2uah_9 + k^2a + k^3 = 0, \tag{14}$$

where

$$k^1 = h_1x + h_2y + h_3, \quad k^2 = 2u(h_7x + h_8y),$$

$$k^3 = -(u^2+v^2)(h_1x + h_2y + h_3).$$

In Eq. (14), the unknowns include h_9 and a, since h_7 and h_8 are already determined as R_{31}/s and R_{32}/s in the previous subsection. Therefore, they can be computed by analytic solution using two pairs of points. Given $n > 2$ pairs, we can have the linear system

$$\boldsymbol{B}\boldsymbol{b} = \boldsymbol{0}, \tag{15}$$

$$\boldsymbol{B} = \begin{bmatrix} k_1^1 & 2u_1 & k_1^2 & k_1^3 \\ \cdots & \cdots & \cdots & \cdots \\ k_n^1 & 2u_n & k_n^2 & k_n^3 \end{bmatrix}$$

and

$$\boldsymbol{b} = [a^2 \quad ah_9 \quad a \quad 1]^{\mathrm{T}}.$$

The solution for the vector $\boldsymbol{b}$ can be obtained up to a scale factor by singular value decomposition. Then we have

$$a = b_1/b_3 \quad \text{and} \quad h_9 = b_2/b_3, \tag{16}$$

where b_i denotes the ith element of $\boldsymbol{b}$.

From the above analysis, the third component of the translation vector, i.e., t_3, is equivalent to sh_9. Therefore, all the variables in the parabolic camera system are recovered analytically.

D. Implementation Procedure

We give a brief procedure for calibrating the parabolic camera system:

(1) Place a planar pattern in the scene. The position is not critical since the system has a very large field of view.
(2) Establish six or more point correspondences between the camera image and the planar pattern.
(3) Construct the coefficient matrix $\boldsymbol{A}$ in (8) and solve it by SVD for the vector $\boldsymbol{h}$.
(4) Recover the motion parameters partially according to (10)–(12).
(5) Construct the coefficient matrix $\boldsymbol{B}$ in (15) and solve it for the mirror parameters and the last component of the translation vector.
(6) Optionally, the solutions are optimized by bundle adjustment using all the point correspondences.

4. EXPERIMENTAL RESULTS

A. Numerical Simulations

We first evaluate the robustness of our algorithm against noise by numerical simulations. We assume that the intrinsic parameters of the camera are known *a priori*. Two cases are considered; calibrating the system when different levels of Gaussian noise are injected, and calibrating the system when it is moving arbitrarily. In both simulations, we use a virtual 5×5 planar pattern and the parameter of the parabolic mirror is set to be $a=0.03$. To evaluate the accuracy quantitatively, the relative errors for the mirror parameter a, the translation vector $\boldsymbol{t}$, and the three rotation angles $\xi=[\alpha,\beta,\gamma]$ are respectively defined as $\|a-\bar{a}\|/\bar{a}$, $\|\boldsymbol{t}-\bar{\boldsymbol{t}}\|/\|\boldsymbol{t}\|$, and $\|\xi-\bar{\xi}\|/\|\xi\|$, where $\bar{a}$, $\bar{\boldsymbol{t}}$, and $\bar{\xi}$ are the estimated values.

In the first simulation, we assumed that the rotation angles and the translation vector of the system were $(\pi/36,\pi/15,\pi/4)$ and $[3\ \ 0.5\ \ 0.05]$, respectively.

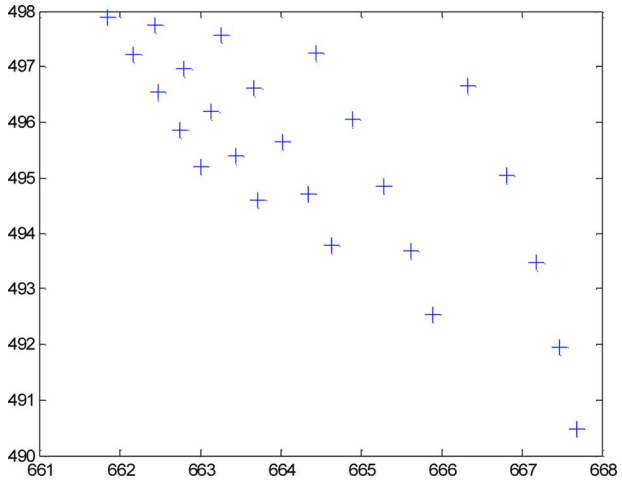

Fig. 2. (Color online) One of the simulated parabolic camera images.

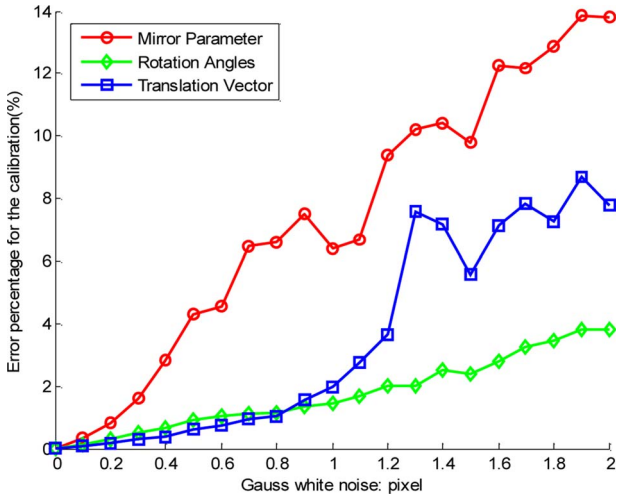

Fig. 3. (Color online) Relative errors versus different levels of noise.

Figure 2 gives one of the simulated parabolic camera images that consisted of 25 image points. Gaussian noise with mean 0 and standard deviation ranging from 0 to 2 pixels was added to those points. Then the proposed calibration algorithm was implemented. At each level of noise, 100 independent runs were performed.

The averaged results are given in Fig. 3, where red circles, green diamonds, and blue squares, respectively, represent the relative errors for the mirror parameter, the rotation angles, and the translation vector. We can see that the error percentages are almost linear with increasing noise and within a reasonable range. Hence, the proposed algorithm is valid and robust to noise.

In another simulation, we changed the rotation angles and the translation vector randomly to simulate arbitrary motion of the system. Obviously, the calibration results were accurate if no noise was added. In order to test the stability of our method, a fixed noise level of 1 pixel was applied to the image points. Table 1 gives the calibration results of five different positions of the system. From these simulations, we can see that the algorithm performs stably when the system undergoes arbitrary motion.

B. Real Data Experiments

The system involved in the real data experiments was built using off-the-shelf components, as illustrated in Fig. 4. The CCD camera was EC1380 with image resolution of 1360×1024 pixels. The parabolic mirror was provided by ACCOWLE Vision Company.

When working, the parabolic camera system can be held by hand since the proposed algorithm has no specific

Table 1. Relative Error Percentage in Cases of Arbitrary Motions

Trial	Mirror Parameter	Rotation Angle	Translation Vector
1	8.0334	1.6067	4.7357
2	6.3702	1.6798	4.4499
3	9.8229	2.4970	6.7023
4	7.6939	1.9456	4.2882
5	7.8479	2.8412	5.2104

Fig. 4. (Color online) System setup in real data experiments.

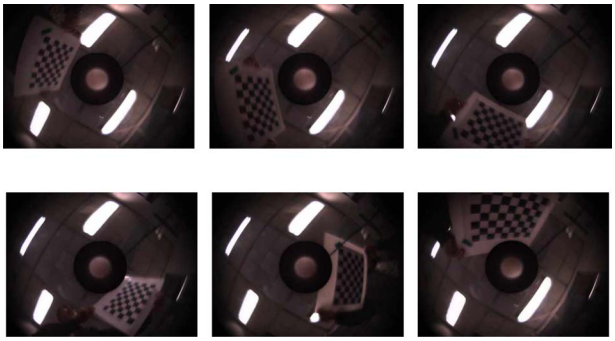

Fig. 5. (Color online) Pattern in six different positions: they are labeled 1–6 from left to right and from top down in this experiment.

requirement of movement. In this experiment, we arbitrarily moved the planar pattern around the system, then calibrated the system and tracked the motion using our algorithm. The pattern was printed on A4 paper. Figure 5 shows images of the pattern in six different positions. The intrinsic parameters of the camera were estimated using the Camera Calibration Toolbox for Matlab [25] before setting up the system. Then the mirror parameter and motions of the pattern were computed using our algorithm. Figure 6 illustrates the reconstructed positions of the pattern in the six positions with the calibration results.

We also reprojected those points of the pattern into the images and calculated the distances between the reprojected points and the corresponding image points in the 2D image space. Table 2 gives the mean and standard deviations of the distances. We can see that the calibration accuracy is acceptable. These experiments further demonstrate the validity of the proposed algorithms quantitatively and qualitatively.

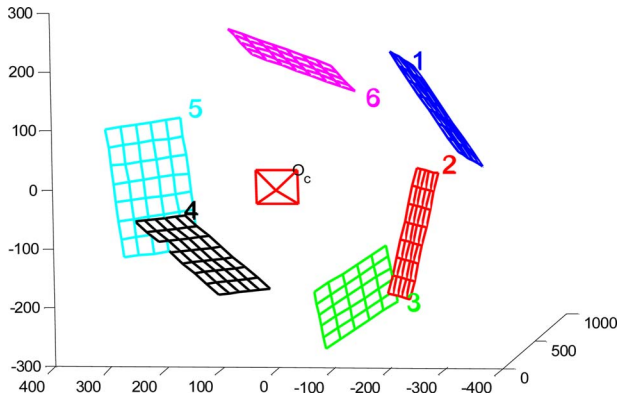

Fig. 6. (Color online) Reconstructed positions of the pattern.

Table 2. Reprojection Errors in the Image Space (Pixels)

	u Component		*v* Component	
Item	Mean	Std. Dev.	Mean	Std. Dev.
1	0.5364	0.4113	0.8448	0.5701
2	0.5446	0.4038	1.0718	0.9099
3	0.5783	0.3651	0.6022	0.8175
4	0.6690	0.4956	0.7050	0.5234
5	0.7529	0.6596	0.9836	0.7769
6	1.1602	0.7797	0.5384	0.4908

5. CONCLUSIONS

We have reported a calibration method for a central parabolic camera system based on the homographic matrix. In this method, the mirror parameter and the motion parameters of the system can be estimated from a closed-form solution assuming that the intrinsic parameters are known. The robustness of the algorithm is enhanced via the use of two over-constrained systems. Hence this algorithm is simple and easy to implement. Both numerical simulations and real data experiments show that the method is accurate and stable for different motions. In many applications, e.g., robot navigation and motion tracking, the motion parameters need to be calibrated frequently and a larger field of view is preferred. In these cases, the proposed method provides a good solution.

ACKNOWLEDGMENT

The work described was fully supported by a grant from the Research Grants Council of Hong Kong (project CityU117106).

REFERENCES

1. B. Zhang and Y. F. Li, "Dynamic calibration of the relative pose and error analysis in a structured light system," J. Opt. Soc. Am. A **25**, 612–622 (2008).
2. B. Zhang, Y. F. Li, and Y. Wu, "Self-recalibration of a structured light system via plane-based homography," Pattern Recogn. **40**, 1368–1377 (2007).
3. S. Baker and K. Nayar, "A theory of catadioptric image formation," Int. J. Comput. Vis. **35**, 175–196 (1999).
4. C. Geyer and K. Daniilidis, "Catadioptric projective geometry," Int. J. Comput. Vis. **45**, 223–243 (2001).
5. P. Barreto, "A unifying geometric representation for central projection systems," Comput. Vis. Image Underst. **103**, 208–217 (2006).
6. X. Ying and Z. Hu, "Can we consider central catadioptric cameras and fisheye cameras within a unified imaging model," in *Proc. European Conference on Computer Vision (ECCV04)* (Springer-Verlag, 2004), Vol. 1, pp. 442–455.
7. Y. H. Wu, Y. F. Li, and Z. Y. Hu, "Easy calibration for para-catadioptric-like cameras," in *IEEE/RSJ International Conference on Intelligent Robots and Systems* (IEEE, 2006), pp. 5719–5724.

8. C. Geyer and K. Daniilidis, "Catadioptric camera calibration," in *IEEE Proc. of the Seventh International Conference on Computer Vision* (IEEE, 1999), Vol. 1, pp. 398–404.
9. P. Barreto and H. Araujo, "Issues on the geometry of central catadioptric image information," in *IEEE Conference on Computer Vision and Pattern Recognition* (IEEE, 2001), pp. 422–427.
10. C. Mei and E. Malis, "Fast central catadioptric line extraction, estimation, tracking and structure from motion," in *IEEE/RSJ International Conference on Intelligent Robots and Systems* (IEEE, 2006), pp. 4774–4779.
11. C. Geyer and K. Daniilidis, "Paracatadioptric camera calibration," IEEE Trans. Pattern Anal. Mach. Intell. **24**, 687–695 (2002).
12. P. Barreto and H. Araujo, "Geometric properties of central catadioptric line images and their application in calibration," IEEE Trans. Pattern Anal. Mach. Intell. **27**, 1327–1333 (2005).
13. P. Barreto and H. Araujo, "Paracatadioptric camera calibration using lines," in *IEEE Proc. of the Ninth International Conference on Computer Vision* (IEEE, 2003), Vol. 2, pp. 1359–1365.
14. P. Barreto and K. Daniilidis, "Unifying image plane liftings for central catadioptric and dioptric cameras," presented at the Workshop on Omnidirectional Vision, Camera Networks and Non-Classical Cameras, Prague, Czech Republic, May 2004.
15. R. Orghidan, E. Mouaddib, and J. Salvi, "Omnidirectional depth computation from a single image," in *IEEE Proc. of International Conference on Robotics and Automation* (IEEE, 2005), pp. 1222–1227.
16. G. Aliega, "Accurate catadioptric calibration for real-time pose estimation in room-size environments," in *IEEE Proc. of the Ninth International Conference on Computer Vision* (IEEE, 2001), Vol. 1, pp. 127–134.
17. Y. H. Wu and Z. Y. Hu, "Geometric invariants and applications under catadioptric camera model," in *IEEE Proc. of the 10th International Conference on Computer Vision* (IEEE, 2005), pp. 1547–1554.
18. S. B. Kang, "Catadioptric self-calibration," in *IEEE Proc. of the Conference on Computer Vision and Pattern Recognition* (IEEE, 2000), Vol. 1, pp. 201–207.
19. C. Geyer and K. Daniilidis, "Structure and motion from uncalibrated catadioptric views," in *IEEE Proc. of the Conference on Computer Vision and Pattern Recognition* (IEEE, 2001), Vol. 1, pp. 279–286.
20. T. Svoboda, T. Padjla, and V. Hlavac, "Epipolar geometry for panoramic cameras," Int. J. Comput. Vis. **49**, 23–37 (2002).
21. J. Barreto and K. Daniilidis, "Epipolar geometry of central projection systems using Veronese maps," in *IEEE Proc. of the Conference on Computer Vision and Pattern Recognition* (IEEE, 2006), Vol. 1, pp. 1258–1265.
22. B. Micusik and T. Pajdla, "Estimation of omnidirectional camera model from epipolar geometry," in *IEEE Proc. of the Conference on Computer Vision and Pattern Recognition* (IEEE, 2003), Vol. 1, pp. 485–490.
23. B. Micusik and T. Pajdla, "Structure from motion with wide circular field of view cameras," IEEE Trans. Pattern Anal. Mach. Intell. **28**, 1135–1149 (2006).
24. B. Micusik and T. Pajdla, "Omnidirectional camera model and epipolar geometry estimation by RANSAC with bucketing," *Lecture Notes in Computer Science* (Springer-Verlag, 2003), pp. 83–90.
25. J. Y. Bouguet, Camera Calibration Toolbox for Matlab, http://www.vision.caltech.edu/bouguetj/calib-doc/, public domain internet software.